Phase diagram of a tubular vesicle adhering between two parallel rigid planes

Xiaohua Zhou,[1,2] Shumin Zhao,[1] Xiaobo Zhai,[3] Kai Zhang,[1] Huawei Chen,[1] and Shengli Zhang[1,*]

[1]*Department of Applied Physics, Xi'an Jiaotong University, Xi'an 710049, People's Republic of China*

[2]*Department of Radiation Biology, Fourth Military Medical University, Xi'an 710032, People's Republic of China*

[3]*College of Science, Xi'an University of Science and Technology, Xi'an 710054, People's Republic of China*

(Received 23 April 2015; revised manuscript received 3 February 2016; published 11 April 2016)

In this study, we propose a two-dimensional (2D) theoretical model to explore the adhesion behavior of a tubular vesicle adhering between two rigid planes, which are constrained by a couple of forces. Based upon the free-energy functional of the system, the equations for the equilibrium shape are derived. The general solution for the system with zero pressure is obtained analytically and the stability of the corresponding equilibrium shapes is tested by numerical simulation. With the volume constraint, three kinds of typical stable shapes are obtained through scanning the parameter space numerically. The phase diagram is obtained and it is occupied mostly by nonsymmetrical shapes. The force-displacement curves obtained for our model are in agreement with experimental results. The catastrophe of force is found at a critical state, which reveals a huge expanding force will act on the two planes by the vesicle. It also implies that vesicles can spontaneously squeeze into a slit only due to adhesion.

DOI: 10.1103/PhysRevE.93.042801

I. INTRODUCTION

When the membrane proteins are ignored, cell membranes that are composed mostly by two layers of phospholipids can be taken as liquid vesicles as well as 2D surfaces. The equilibrium shapes of vesicles can be described by the Helfrich-Canham bending energy theory [1–4]. In the past 40 years, the shapes and deformations of artificial vesicles, which often have single component, were widely studied and many theoretic results are in accordance with experimental observations, such as the Clifford torus [5–7] and the beyond-Delaunay surface [8,9]. Also, the Helfrich-Canham bending energy theory has been developed extensively to deal with the equilibrium shapes of open vesicles [10], vesicle adhesion systems [11–13], multicomponent vesicles [14,15], cell membranes with cross-linking structures [16], and so on [17]. However, the dynamic characteristics, such as the viscoelasticity, of cell membranes resulting from the membrane protein cross-linker are beyond the Helfrich-Canham bending energy theory. In recent years, many studies have focused on the viscoelasticity of single cells [18–21]. In these works, the cells are adhered between two paralleled plates and the dynamic behaviors are investigated by changing the mechanical environment. It should be noted that the cell membranes are complex structures, which means the protein cross-linker and the two layers of phospholipids codetermine the mechanical properties of cell membranes. Although the works in Refs. [18–21] have explored the protein cross-linker, it lacks a similar study about the liquid bilayer vesicles. So if a vesicle adheres between two plates, what kind of mechanical phenomena will appear is still unknown.

To study the vesicle adhesion systems, Seifert and Lipowsky [11–13] initially introduced the contact potential in the Helfrich-Canham bending energy theory to describe the intensity of the adhesion energy between a vesicle and a substrate. Their results indicate that the equilibrium structures result from the competition between the curvature elastic energy and the adhesion energy. Deserno *et al.* [22] developed a general geometrical framework to study the fluid surface adhesion. The equilibrium shape equations for the contact boundary line obtained by them are widely applicable.

Although much effort has been performed to study the equilibrium structures of vesicle adhesion systems, we still need a deep understanding on the mechanical characteristics, especially how these adhesion structures can be disintegrated by physical methods, such as by pulling force [23–25]. In other words, when adhesion becomes a negative effect, how to eliminate it requires further study. The work in Ref. [24] provided some useful information. However, we notice that this work didn't consider the volume constraint for each vesicle (the pressure always is zero in their work). So, whether the volume constraint can induce new mechanical behavior is unknown. Recently, Steffen *et al.* [26] studied the depletion-induced adhesion of red blood cells. They provided the relationship between the force and the distance when using force to separate two adhered blood cells and said that is needed in theoretical investigations. Although previous theoretical works in Refs. [23,24] have studied similar questions as the model in Ref. [26], their results about the force-distance curves cannot explain the experimental data in Ref. [26]. What causes the force-distance relationship is still challenging.

Motivated by the above analysis, in this work we propose a 2D model to explore the adhesion behavior of a tubular vesicle adhering between two rigid planes, which are constrained by a couple of forces. In Sec. II, the equilibrium shape equations are derived and the general solution in the zero pressure case is derived analytically. In Sec. III, the phase diagram for the vesicle with fixed volume is obtained through scanning the 3D parameter space numerically and all shapes are tested by stability analysis. Finally, these results are recapped in a short discussion in Sec. IV.

II. SHAPES WITH NO VOLUME CONSTRAINT

In the Helfrich-Canham bending energy theory, the free energy for vesicle is [1,2]

$$E = \frac{1}{2}\kappa \oint (K_1 + K_2)^2 dS + \kappa_c \oint K_1 K_2 dS, \qquad (1)$$

*zhangsl@mail.xjtu.edu.cn

where K_1 and K_2 are two principal curvatures, κ is the bending rigidity, κ_c is the modulus of elasticity for Gaussian curvature, and dS is the area element. For closed shapes, the second term in Eq. (1) satisfies the Gauss-Bonnet theorem $\oint K_1 K_2 dS = 2\pi E_r$ [27], where E_r is the Euler characteristic which only depends on the topological structure of the surface. For spherical topology surface, $E_r = 2$. For torus, cylinders, and tubes with infinite length, $E_r = 0$. In the following text, we will study the tubes with infinite length, so the valid total free energy is reduced to $E = \frac{1}{2}\kappa \oint (K_1 + K_2)^2 dS$. Considering the volume and surface constraints, the energy functional is $E_t = E + p \oint dV + \gamma \oint dS$, where p is the pressure difference between the outside and inside of the vesicle, γ is the surface tension coefficient, and dV is the element of volume. The equilibrium shape equation can be obtained by discussing the first variation $\delta E_t = 0$ [3]. In 2D case, one principal curvature is zero and the valid free energy is reduced to $E = \frac{1}{2}\kappa \oint K^2 ds$, where K is the curvature and ds is the element of the arc length of vesicle. If a 2D vesicle adheres to a rigid plane [11], the total free energy is changed to $E = \frac{1}{2}\kappa \oint K^2 ds - \omega L_d$, where ω is the adhesion potential and L_d is the total adhesion length.

Figure 1 is the cross section of a tubular vesicle adhered between two parallel rigid planes. A couple of forces perpendicularly act on them and keep a stable distance D between them. This system can be simplified as a 2D model. The contact red lines stand for the adhesion regions and the curved blue parts are free ones. The equilibrium shape is governed by the competition between the curvature elastic energy and adhesion energy.

First, we consider that there is no volume constraint, which means the pressure is zero. In this case, we can make an ansatz that the shape has D_2 symmetry. (This hypothesis will be confirmed by simulation later in text). Then the two free parts are equal and we can only choose half of the lower part

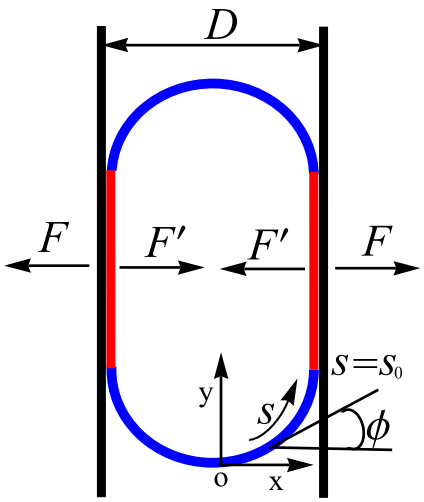

FIG. 1. A tubular vesicle adheres between two parallel rigid planes. A couple of forces F perpendicularly act on them and keep them within the distance D. The forces that the vesicle acts on the two planes are F and we have $F' = -F$. The positive F' refers to the vesicle pulling the walls together, and the negative F' corresponds to the vesicle pushing them apart. The contact red parts are adhesive regions, and the curved blue parts are free.

to study. As shown in Fig. 1, the system is defined in the x-y plane and the bottom point is the initial point at which the arc length $s = 0$. At the initial adhesion point, there is $s = s_0$. Let ϕ be the angle between the tangent of the free arc and the x axis, the curvature is $K = d\phi/ds = \dot{\phi}$. The total free energy of the whole system is $E = 2\kappa \int_0^{s_0} \dot{\phi}^2 ds - 2\omega B$, where B is the length of one adhesion part. Considering the volume constraint (the surrounding area in the 2D case) and surface constraint (the total length in the 2D case), the corresponding Lagrange functional is [11]

$$\Pi = E + \int_0^L [px \sin\phi + \lambda(\dot{x} - \cos\phi)] ds, \tag{2}$$

where $L = \oint ds$ is the total length, and λ is the Lagrange coefficient. The shape equations for the free part are [28]

$$\kappa\ddot{\phi} - px\cos\phi - \lambda\sin\phi = 0, (0 < s < s_0), \tag{3}$$
$$p\sin\phi - \dot{\lambda} = 0, (0 < s < s_0). \tag{4}$$

The corresponding geometrical constraint equations are

$$\dot{x} = \cos\phi, \dot{y} = \sin\phi. \tag{5}$$

The fixed boundary conditions can be described as

$$\phi(0) = 0,\ x(0) = 0,\ y(0) = 0, \tag{6}$$
$$\phi(s_0) = \pi/2,\ x(s_0) = D/2. \tag{7}$$

At the point $s = s_0$, there is the condition [11,22,24]

$$2\omega = \kappa\dot{\phi}^2|_{s=s_0}. \tag{8}$$

In order to obtain dimensionless results, we choose $L = 2\pi$ and $\kappa = 1$ (see details in the appendix for reasons). When there is no volume constraint, we have $p = 0$. Then the shape Eqs. (3) and (4) are reduced to [28]

$$\dot{\phi}^2 = 2\lambda(C - \cos\phi), \tag{9}$$

where C is an integral constant. It yields

$$ds = \frac{d\phi}{\sqrt{2\lambda(C - \cos\phi)}}. \tag{10}$$

The distance can be written as

$$D = 2\int_0^{s_0} \cos\phi ds = \int_0^{\pi/2} \frac{2\cos\phi d\phi}{\sqrt{2\lambda(C - \cos\phi)}}. \tag{11}$$

Using Eq. (10) and $L = 2\pi = 4s_0 + 2B$, we derive

$$B = \pi - 2\int_0^{\pi/2} \frac{1}{\sqrt{2\lambda(C - \cos\phi)}} d\phi. \tag{12}$$

The total free energy is

$$E = 2\int_0^{\pi/2} \sqrt{2\lambda(C - \cos\phi)} d\phi - 2\omega B. \tag{13}$$

Making use of Eq. (9), condition Eq. (8) is reduced to

$$\omega = \lambda C. \tag{14}$$

Substituting it into Eqs. (11), (12), and (13), and defining $F[x, y]$ and $S[x, y]$ as the first and second incomplete elliptical

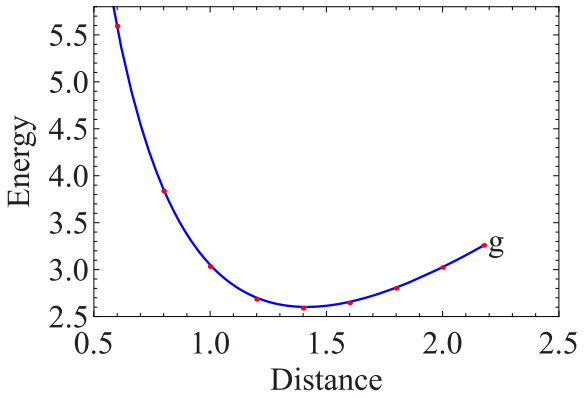

FIG. 2. The energy-distance relationship with $\omega = 1$. The energy has the minimum at the distance $D = \sqrt{2}$. At the point g, D reaches its maximal value $D_m = 2.177$, and after that the adhesion will vanish. The solid line is the analytical result and the red points are obtained by simulation.

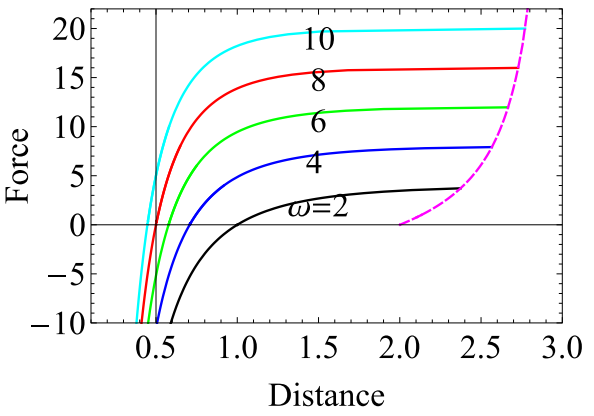

FIG. 3. The force-distance relationships for different ω. The dotted purple line is the adhesion vanishing line on which the force reaches its maximum (pull-off force).

integral, respectively, we obtain

$$D = 2\sqrt{\frac{2C}{\omega(C-1)}}\left\{C \times F\left[\frac{\pi}{4}, \frac{2}{1-C}\right] - (C-1) \times S\left[\frac{\pi}{4}, \frac{2}{1-C}\right]\right\}, \quad (15)$$

$$B = \pi - 2\sqrt{\frac{2C}{\omega(C-1)}} \times F\left[\frac{\pi}{4}, \frac{2}{1-C}\right], \quad (16)$$

$$E = 4\sqrt{\frac{2\omega(C-1)}{C}} \times S\left[\frac{\pi}{4}, \frac{2}{1-C}\right] + 4\sqrt{\frac{2\omega C}{(C-1)}} \times F\left[\frac{\pi}{4}, \frac{2}{1-C}\right] - 2\pi\omega. \quad (17)$$

If ω is given, there is only one parameter C in the above expressions. So, for each ω, one can express the relationship between the total energy E and the distance D using the parametric curve $[E(C), D(C)]$. In Fig. 2 it shows the curve of E and D with $\omega = 1$, we can see there is an optimal distance at which the total energy has the minimal value. Letting

$$\frac{dE}{dD} = \frac{dE/dC}{dD/dC} = 0, \quad (18)$$

we find it needs $C \to \infty$. Then, there is

$$\dot{\phi}^2 = 2\lambda(C - \cos\phi) = 2\omega(C - \cos\phi)/C = 2\omega. \quad (19)$$

This result indicates the optimal shape of the free parts in Fig. 1 are two half of circles with the same radius $R = \sqrt{1/(2\omega)}$. The minimal energy is $E_m = 2\pi(\sqrt{2\omega} - \omega)$.

If the two planes in Fig. 1 are constrained by a couple of forces and the system is balanced, the forces satisfy

$$F = \frac{dE}{dD} = \frac{dE/dC}{dD/dC}. \quad (20)$$

We show the parametric curves $[F(C), D(C)]$ in Fig. 3 for different ω, which are similar to the results in Ref. [24] that the maximal force occurs at the adhesion vanishing point. Under the action of the couple of forces, if the distance D exceeds the maximal value D_m, the adhesion length between the vesicle and the planes will vanish. Letting $B = 0$ in Eq. (16), it yields $\omega = \omega(C)$. Substituting it into Eq. (15), we obtain the maximal distance $D_m = D_m(C)$. We show the curve of D_m and ω in Fig. 4. Actually, the adhesion vanishing point g in Fig. 2 and the adhesion vanishing line in Fig. 3 are derived by this way. If there is no adhesion and the vesicle is free, it will be a circle with the radius $R = 1$. So if the distance $D < 2$, the adhesion will occur because the vesicle must contact with two planes. Contrarily, the adhesion vanishing distance must satisfy $D_m > 2$, which yields $\omega > 0.5$. This result is first presented by Seifert [11].

III. SHAPES WITH THE VOLUME CONSTRAINT

In the former section, we studied the adhesion behavior of a tubular vesicle adhering between two rigid planes. Supposing the shapes have D_2 symmetry, we obtained the analytical results under no volume constraint. In this section we will prove that our former results are reliable and further investigate the nonzero pressure state with volume constraint by simulation.

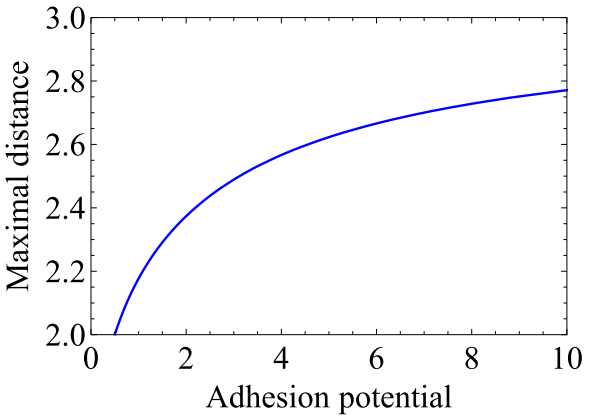

FIG. 4. The curve of the maximal distance D_m vs. ω.

When there is volume constraint, it is difficult to solve the shape Eqs. (3) and (4) analytically. Here we use the finite elemental software *Surface Evolver* [29] to study the adhesion system. This software has been generally used to simulate the equilibrium shapes of singular vesicles [30–32], vesicle adhesion systems [33], and plate adhesion structures [34]. In this software, the total energy functional for the model in Fig. 1 is

$$E_t = m \oint K^2 ds - \omega L_d + p \iint_L d\sigma + \gamma \oint ds, \quad (21)$$

where m is an adjustable constraint and σ is the area surrounded by the vesicle. Similar to the study in the former section, we set $m = 1/2$ and $L = 2\pi$ in the simulation and the dimensionless parameter can be defined (see the Appendix). Considering the volume constraint, we define the reduced volume $v = \frac{1}{\pi}\int\int_L d\sigma$, which can be adjusted in simulation. Furthermore, the two rigid planes are added in simulation as boundary conditions and the distance between them is adjustable. Based on the above methods and techniques, each equilibrium state is determined by the three parameters: ω, v, and D. So, the corresponding phase diagram should be three dimensional.

Before studying the phase diagram, we tested our former results with $p = 0$. The red points in Fig. 2 are obtained by simulation, which are in good agreement with our analytical results. Moreover, the stability analysis is important for each equilibrium shape. In order to estimate the stability, the so-called *Hessian* needs to be studied, which is the matrix of the second differential coefficients of the total free energy and can be calculated numerically by the *Surface Evolver*. If the shape is stable, it must have a positive definite *Hessian* matrix. Making use of this method, we tested our former results and found all of them are stable and have D_2 symmetry.

In the former discussion, we suppose the two planes are big enough and the whole vesicle is clipped within the two planes. In this case, with fixed v one can deduce the shape reaches the threshold that the free parts are two half circles with the same radii, then the distance reaches its minimum $D = D_s$ and cannot decrease any more. There is

$$D_s = 2(1 - \sqrt{1 - v}). \quad (22)$$

If this critical shape is a solution of the shape Eqs. (3) and (4), the condition in Eq. (8) should be satisfied and it gives the radii of the free parts of this critical shape $R_s = \sqrt{1/2w}$. Considering $D_s = 2R_s$, we have

$$v = \sqrt{2/\omega} - 1/(2\omega). \quad (23)$$

This is the condition for the critical shape to be a solution of the shape Eqs. (3) and (4). Moreover, the general equilibrium equations for free vesicles were discussed by Ou-Yang *et al.* in Refs. [35,36]. Making use of their results we obtain the following additional condition for this critical shape,

$$pR_s^3 + \gamma R_s^2 - \kappa/2 = 0. \quad (24)$$

We tested this condition by the *Surface Evolver* and found the numerical results are confirmed by it.

However, if the two planes are not big enough and the vesicle adheres to the borders of the two planes, new shapes will appear and it allows the distance $D < D_s$. An example in Fig. 5 shows that one plane is not big enough and the distance $D < D_s$. In our simulation, we don't constrain the length of the two rigid planes and set only the distance D between the two adhesion lines as a constraint, which allows us to explore the whole region of D and easily stride across the critical value $D = D_s$.

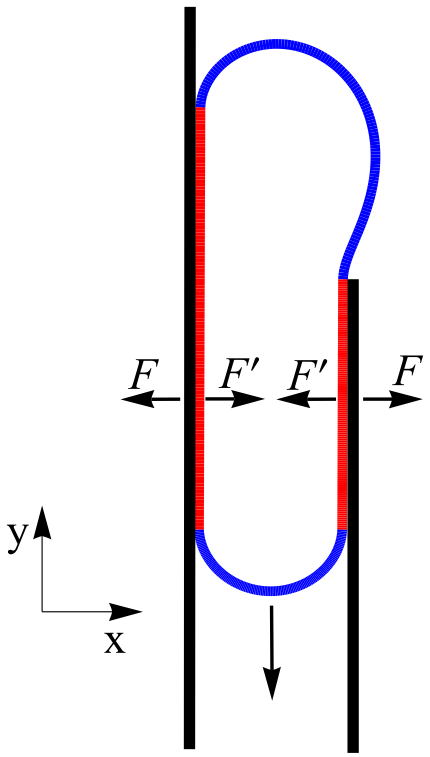

FIG. 5. A tubular vesicle with fixed volume adheres between two parallel rigid planes. One plane is not big enough and the distance D between them satisfies $D < D_s$.

Through scanning the parameter space, three kinds of typical shapes are found. A set of examples are shown in Fig. 6. These shapes have the same contact potential $\omega = 10$ and reduced volume $v = 0.8$. Figure 6(a) shows a nonsymmetrical shape with $D = 1 < D_s$. When $D > D_s$ there is another kind of nonsymmetrical shape as shown in Fig. 6(b). Moreover, a kind of symmetrical shape like Fig. 6(c) is found when

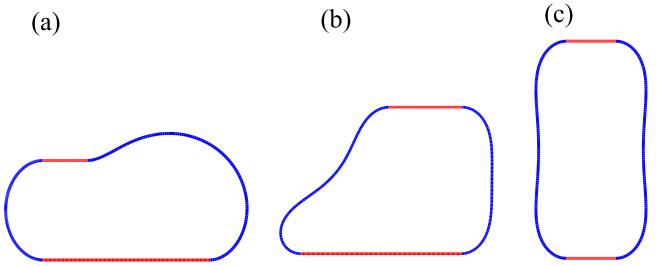

FIG. 6. Three typical shapes with the same adhesion potential $\omega = 10$ and reduced volume $v = 0.8$. (a) A nonsymmetrical shape (phase I) with $D = 1$. (b) A nonsymmetrical shape (phase II) with $D = 1.5$. (c) A D_2 symmetrical shape (phase III) with $D = 2.3$.

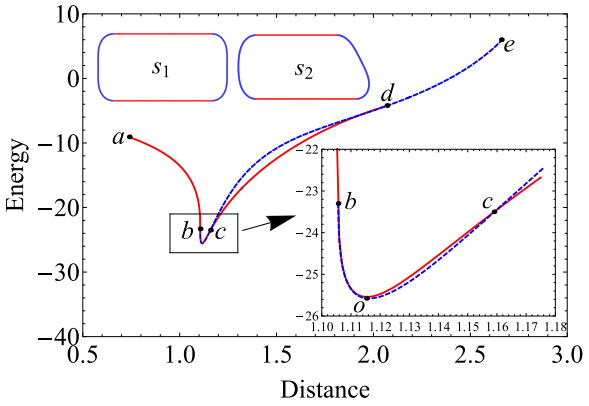

FIG. 7. The energy-distance bifurcation between three phases at $\omega = 10$ and $\nu = 0.8$. The dotted blue line is the D_2 symmetrical phase like Fig. 6(c). As to the solid red line, from point a to b it is the nonsymmetric phase in Fig. 6(a) and from point b to d it is the nonsymmetric phase in Fig. 6(b). At the points a ($D = 0.74$) and e ($D = 2.66$), one adhesion part of each shape will reduce to zero. Point b is the critical state with $D = 1.1056 \simeq D_s$, and point o is the lowest energy point with $D = 1.116$. Point d is a symmetry breaking point with $D = 2.07$. At the crosspoint c with $D = 1.159$, the energy of two phases is degenerate. The inside shapes s_1 and s_2 are the two phases at the degeneracy point c.

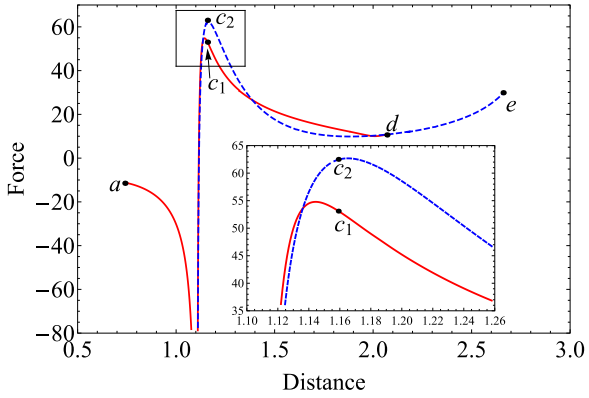

FIG. 8. The force-distance curves at $\omega = 10$ and $\nu = 0.8$. At point $D = D_s = 1.1056$, the force $F \to -\infty$. The dotted blue line is the phase III with D_2 symmetry. The two solid red lines are the nonsymmetric phases: phase I for $D < D_s$ and phase II for $D > D_s$. The a, d, and e points correspond to the a, d, and e points in Fig. 7, respectively. The c_1 and c_2 points correspond to the degeneracy point c in Fig. 7. Simulation reveals the shape will drop from point c_2 to c_1 when we increase D from an initial value $D < D_s$.

$D > D_s$. The lowest energy state always occurs when D narrowly exceeds D_s.

Figure 7 shows the energy-distance bifurcation between three phases at $\omega = 10$ and $\nu = 0.8$. Two phases are nonsymmetric shapes and another has the D_2 symmetry. When $D < D_s$ there is no stable symmetric shapes and only has one nonsymmetric phase (phase I). When $D > D_s$ there is a symmetric phase (phase III) and a nonsymmetric phases (phase II) and they cross at the point c. Point d is the symmetry breaking point and there is only the phase III above it. From this figure we can see that, between points c and d, the phase II has lower energy than the phase III. The inside figure indicates the lowest energy point o with $D = 1.116$ has D_2 symmetry. Now, we know the points b, c, and d are phase transition points, but to identify the orders of them requires following additional discussion.

Figure 8 gives the relationship between the force $F = dE/dD$ and the distance D. It shows the force has a catastrophe point at $D = D_s$ (simulation indicates $F \to -\infty$ at this point). When $D < D_s$, the force is always negative. When $D > D_s$, the forces of the phases II and III all will rapidly increase to their maximal values. The points c_1 and c_2 correspond to the energy degeneracy point c in Fig. 7. Clearly, Fig. 8 shows the forces of the two phases are unequal at these two points. From the inside figure we can deduce that the values of dF/dD also are not equal at these two points (one is positive and the other is negative). Thus, point c in Fig. 7 is a first-order phase transition point. When we increase D from an initial value $D < D_s$, simulation reveals the shape will evolve along the phase II until it reaches point c_2. Then it will drop to point c_1 if there is a small perturbation. At point d, the forces between the two phases seem to be continuous. We also studied the relationship between dF/dD and D at this point. Based on the accuracy of the simulation software, we only know it is a possible second-order or higher-order phase transition point but cannot identify it.

Most impressively, when we increase D from an initial value $D < D_s$, Fig. 8 indicates an expanding force will act on the planes by the vesicle and it will become huge nearby $D = D_s$. Looking back to Fig. 5, where the vesicle adheres between two planes and the distance $D < D_s$. If the planes are not fixed on the x direction, according to Figs. 7 and 8, the vesicle will push the two planes away and squeeze into the slit. This process is shown in Fig. 9, where one plane is fixed and the other is connected with a spring. Supposing that the shape in Fig. 9(a) is at the pint a in Fig. 7 and the spring is in the original length, Fig. 8 reveals there will be a couple of pushing forces acting on the two plates by the vesicle. Then the plate on the right-hand side of Fig. 9(a) will be pushed away and shape will roll down from the high-energy point a toward the lowest energy point o. But the elastic force acting on the plate by the spring will increase with the increase of the distance D. So, when the pushing force by the vesicle and the elastic force by the spring strike a balance on the right plate, the shape of vesicle will not change and form Fig. 9(b), where we can see the vesicle moves into the slit with a definite length. It must be pointed out that due to the only stable phase when $D < D_s$ is nonsymmetric, the above processes need the edge of one plate to exceed the edge of the other with an enough length.

Figure 10 shows the phase diagram of $\omega = 10$. From it we can see a large area is occupied by nonsymmetric shapes. For instance, at $\nu = 0.6$, there is no stable symmetric shape. Figure 11 shows the energy-distance curves with $\omega = 10$ and $\nu = 0.6$. Besides the former two nonsymmetric phases (phase I and phase II), there is a new nonsymmetric phase (phase IV, see the red branch in the inside figure of Fig. 11). But this new branch is metastable because its energy is always higher than phase II. It is found that this branch begins at the critical point $D = D_s$ and finally converges to phase II. The force-distance curves in Fig. 12 reveal there is the catastrophe of force at the critical point $D = D_s$. If we increase D crossing

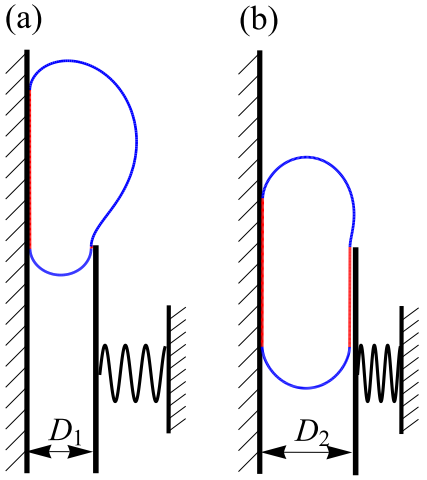

FIG. 9. A vesicle squeezes into a slit due to adhesion. (a) The left plate is fixed and the right plate only can move along the horizontal direction. The spring is fixed on the right plate and is in the original length. The total free energy of the structure is at the critical point a in Fig. 7, where the adhesion on the right plate is just beginning. According to Fig. 8, the vesicle will push away the right plate and the shape will roll down from the high energy state (point a in Fig. 7) toward the lowest energy state (point o in Fig. 7). (b) When the pushing force by the vesicle and the elastic force by the spring strike a balance on the right plate, the shape of vesicle will not change and then we can see the vesicle moves into the slit with a definite length.

D_s, simulation indicates the shape always evolves along the metastable phase IV until it converges to the phase II. There are likely two reasons for this phenomenon. First, when the shape drops from D_s^- to D_s^+, it will first touch the phase IV due to its higher energy. Second, there is a small energy barrier between phases II and IV, which hinders the phase IV to drop into phase II if the perturbation is not big enough. Phase IV has a special feature in that the force has an evident trough, such as the point n in Fig. 12. More results are shown in Fig. 13 and

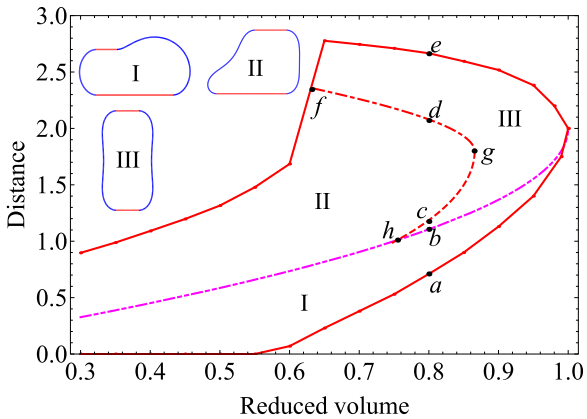

FIG. 10. The phase diagram at $\omega = 10$. The solid red line is the adhesion vanishing boundary line and the dotted line from point h to g is the first-order phase transition line. The dotted dashed line from point g to f is the symmetry breaking line. The double dotted dashed line is the critical state in Eq. (22). The a, b, c, d, and e points correspond to the a, b, c, d, and e points in Fig. 7, respectively.

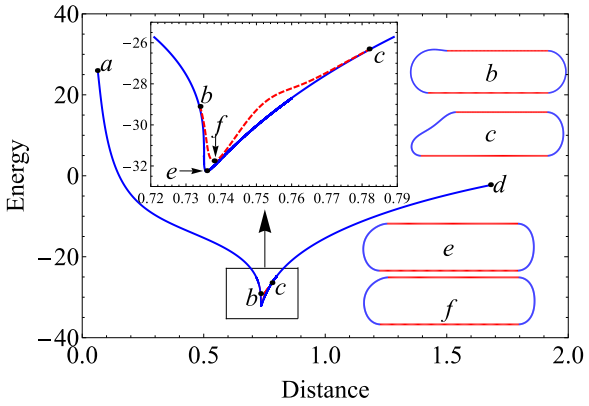

FIG. 11. The energy-distance curves at $\omega = 10$ and $\nu = 0.6$. The dotted red branch is the phase IV, which begins at the critical point b with $D = D_s = 0.735$ and finally converges to the phase II at point c. Points e and f are two lowest energy states for phases II and IV, respectively. The inset shapes b, c, e, and f are corresponding to the points b, c, e, and f, respectively. When decreasing the simulation step length, points e and f will get closer to point b.

we can also see the force fluctuation for phase IV. Particularly, even when Eq. (23) is satisfied, the curve with $\omega = 3.7013$ in Fig. 13 reveals that there also is the catastrophe of force at $D = D_s$ and force fluctuation when D accessing D_s a little. We think these phenomena are possible to be uncovered in future experiments.

The curves for pase II in Fig. 13(b) obtained by decreasing D show that the force F will reach its maximum rapidly when D is increased from $D_s = 0.735$. This rapid increase is due to a very narrow valley for the total energy, such as the results in Fig. 11. When we increase D, before the shape can climb out of this narrow valley, the force will increase rapidly due to the fast increase of the free energy. After that, the increasing speed of its free energy will slow down and consequently the force F monotonously decreases with increasing D until one adhesion part is failed. The right end point of each line is the

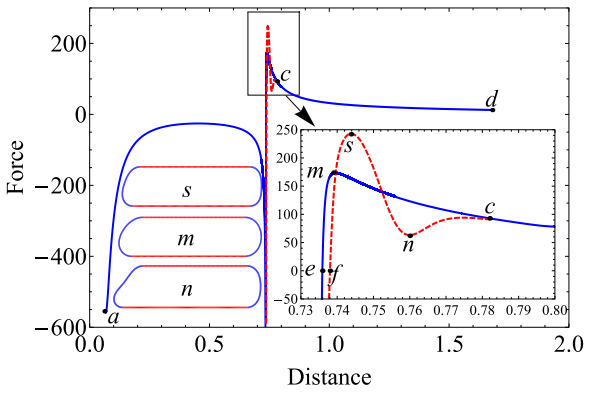

FIG. 12. The force-distance relationships at $\omega = 10$ and $\nu = 0.6$. At the singular point $D = D_s = 0.735$, the force $F \to -\infty$. The dotted red line, which is phase IV, has evident undulation. The inset shapes s, m, and n correspond to the local maximum points s, m, and minimum point n, respectively. The points e and f with $F = 0$ correspond to the two lowest energy states e and f in Fig. 11, respectively.

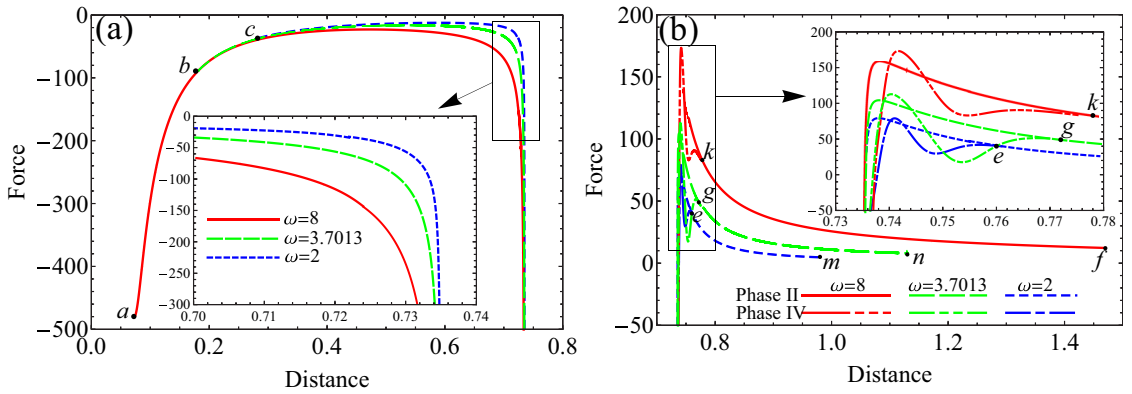

FIG. 13. The force-distance relationships at $v = 0.6$ for different ω. (a) for $D < D_s$ and (b) for $D > D_s$. At the singular point $D = D_s = 0.735$, the forces $F \to -\infty$. a, b, and c are three end points for phase I. e, g, and k are three phase transition points between phase II and phase VI. The lines for phase II with $D > D_s$ are in accordance with the experimental phenomena in Ref. [26].

adhesion vanishing point at which the length of one adhesion part reduces to zero. The above-mentioned phenomena are in good agreement with the experimental results in Fig. 2(b) of Ref. [26]. Figure 14 shows the phase diagram for different ω, which can be taken as the projection of the 3D phase diagram in the v-D plane. In most areas, we can see the lowest energy shape is nonsymmetrical.

IV. CONCLUSIONS

In summary, we have investigated the behavior of a tubular vesicle adhering between two rigid planes, which are constrained by a couple of forces. The analytical configurations without volume constraint are derived and three kinds of typical stable shapes are obtained for the vesicles with volume constraints. The phase diagram of the vesicle with fixed volume is determined numerically, which indicates that, in most areas, the shape is nonsymmetrical. It also implies vesicle could squeeze into a slit only due to adhesion. Although the force-distance relationships are in accordance with the experimental phenomena in Ref. [26], we have to say that our model is only a 2D case, which just provides the similar trend with experimental results qualitatively. Numerical agreement needs a more complete 3D model, which will be studied in our future work.

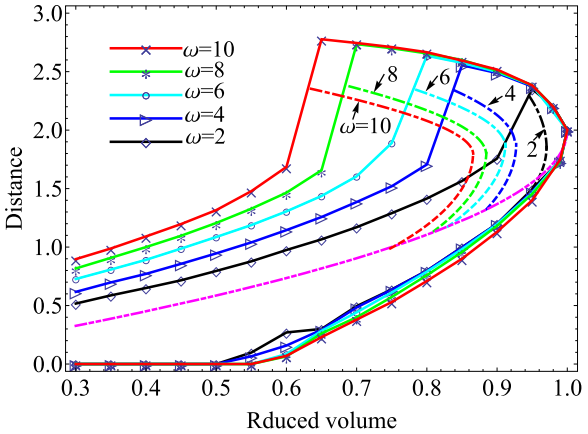

FIG. 14. The phase diagram which can be taken as the projection of the 3D phase diagram in the v-D plane. For each ω, the domain for each kind of shape is similar to Fig. 10. It indicates the nonsymmetrical shapes occupy a larger area than the symmetrical ones.

ACKNOWLEDGMENTS

We would like to thank professor Ken Brakke for his kind help on the use of the *Surface Evolver*. This work is supported by the National Natural Science Foundation of China Grants No. 11304383, No. 11374237, and No. 11504290.

APPENDIX

In this appendix, we show why we will get dimensionless results when choosing $\kappa = 1$ and $L = 2\pi$ for the models in Eqs. (2) and (21). Different vesicles maybe have different size (surface area) and bending rigidity κ. So to study the physical properties of different vesicles, such as the free energy, dimensionless results will be convenient. Let vesicle length $L = \oint ds$ be the length of a circle; the radius of the circle is $R_0 = L/(2\pi)$. Then we can define the following dimensionless parameters: $\tilde{x} = x/R_0$, $\tilde{y} = y/R_0$, $\tilde{s} = s/R_0$, $\tilde{p} = pR_0^3/\kappa$, $\tilde{\lambda} = \lambda R_0^2/\kappa$, $\tilde{\omega} = \omega R_0^2/\kappa$, and $\tilde{\Pi} = \Pi R_0/\kappa$. Substituting these dimensionless parameters into Eqs. (3), (4), and (5) and the conditions in Eqs. (6), (7), and (9), we will obtain dimensionless results by solving them [28]. But there is a simple way to do the above operations and obtain dimensionless results. If we fix $L = \oint ds = 2\pi$ and $\kappa = 1$, there are $R_0 = 1$, $\tilde{x} = x$, $\tilde{y} = y$, $\tilde{s} = s$, $\tilde{p} = p$, $\tilde{\lambda} = \lambda$, $\tilde{\omega} = \omega$, and $\tilde{\Pi} = \Pi$. Then we will get dimensionless results by solving shape Eqs. (6) and (7). Similarly, in Eq. (21) we need to define other dimensionless parameters $\tilde{E}_t = E_t R_0/(2m)$, $\tilde{K} = K R_0$, $\tilde{\omega} = \omega R_0^2/(2m)$, $\tilde{p} = pR_0^3/(2m)$, $\tilde{\gamma} = \gamma R_0^2/(2m)$, $\tilde{V} = V/R_0^2 = (\int \int_L d\sigma)/(R_0^2)$, and the reduced volume $v = \tilde{V}/\pi = (\int \int_L d\sigma)/(\pi R_0^2)$. When choosing $L = \oint ds = 2\pi$ and $m = 1/2$, we have $\tilde{K} = K$, $\tilde{\omega} = \omega$, $\tilde{p} = p$, $\tilde{\gamma} = \gamma$, $V = \tilde{V}$, $v = \frac{1}{\pi} \int \int_L d\sigma$, and dimensionless energy functional $\tilde{E}_t = E_t$. Then the reduced volume satisfies $0 \leqslant v \leqslant 1$, which will make it very convenient to solve the shape equations and study the solutions.

[1] W. Helfrich, Z. Naturforsch. c **28**, 693 (1973).
[2] P. Canham, J. Theor. Biol. **26**, 61 (1970).
[3] O.-Y. Zhong-can and W. Helfrich, Phys. Rev. Lett. **59**, 2486 (1987).
[4] U. Seifert, K. Berndl, and R. Lipowsky, Phys. Rev. A **44**, 1182 (1991).
[5] Z.-c. Ou-Yang, Phys. Rev. A **41**, 4517 (1990).
[6] M. Mutz and D. Bensimon, Phys. Rev. A **43**, 4525 (1991).
[7] B. Fourcade, M. Mutz, and D. Bensimon, Phys. Rev. lett. **68**, 2551 (1992).
[8] R. Bar-Ziv and E. Moses, Phys. Rev. Lett. **73**, 1392 (1994).
[9] H. Naito, M. Okuda, and O.-Y. Zhong-can, Phys. Rev. Lett. **74**, 4345 (1995).
[10] Z. C. Tu and Z.-c. Ou-Yang, Phys. Rev. E **68**, 061915 (2003).
[11] U. Seifert and R. Lipowsky, Phys. Rev. A **42**, 4768 (1990).
[12] R. Lipowsky and U. Seifert, Langmui **7**, 1867 (1991).
[13] U. Seifert, Phys. Rev. A **43**, 6803 (1991).
[14] F. Julicher and R. Lipowsky, Phys. Rev. Lett. **70**, 2964 (1993).
[15] M. Yanagisawa, M. Imai, and T. Taniguchi, Phys. Rev. Lett. **100**, 148102 (2008); Phys. Rev. E **82**, 051928 (2010).
[16] Z. C. Tu and Z.-c. Ou-Yang, J. Phys. A: Math. Gen. **37**, 11407 (2004).
[17] R. Capovilla and J. Guven, J. Phys. A: Math. Gen. **38**, 2593 (2005).
[18] D. Mitrossilis, J. Fouchard, A. Guiroy, N. Desprat, N. Rodriguez, B. Fabry, and A. Asnacios, Proc. Natl. Acad. Sci. USA **106**, 18243 (2009).
[19] D. Mitrossilis, J. Fouchard, D. Pereira, F. Postic, A. Richert, M. Saint-Jean, and A. Asnacios, Proc. Natl. Acad. Sci. USA **107**, 16518 (2010).
[20] J. Fouchard, C. Bimbard, N. Bufi, P. Durand-Smet, A. Proag, A. Richert, O. Cardoso, and A. Asnacios, Proc. Natl. Acad. Sci. USA **111**, 13075 (2014).
[21] J. Etienne, J. Fouchard, D. Mitrossilis, N. Bufi, P. Durand-Smet, and A. Asnacios, Proc. Natl. Acad. Sci. USA **112**, 2740 (2015).
[22] M. Deserno, M. M. Muller, and J. Guven, Phys. Rev. E **76**, 011605 (2007).
[23] W. D. Shi, X. Q. Feng, and H. J. Gao, Acta. Mech. Sin. **22**, 529 (2006).
[24] C. Majidi and K.-T. Wan, J. Appl. Mech. **77**, 041013 (2010).
[25] A. S. Smith, E. Sackmann, and U. Seifert, Europhys. Lett. **64**, 281 (2003).
[26] P. Steffen, C. Verdier, and C. Wagner, Phys. Rev. Lett. **110**, 018102 (2013).
[27] M. P. Do Carmo, *Differential Geometry of Curves and Surfaces* (1st ed., Prentice-Hall, New York, 1976), pp. 264-283.
[28] X. H. Zhou, J. L. Liu, and S. L. Zhang, Colloid Surface B **110**, 372 (2013).
[29] K. Brakke, Exp. Math. **1**, 141 (1992); This software is easily available free of charge from http://www.susqu.edu/facstaff/b/brakke/.
[30] J. Yan, Q. H. Liu, J. Liu, and Z.-C. Ou-Yang, Phys. Rev. E **58**, 6308 (1998).
[31] X. H. Zhou, S. G. Zhang, L. Q. Xie, and F. Zheng, Int. J. Mod. Phys. B **22**, 2769 (2008).
[32] X. Michalet, Phys. Rev. E **76**, 021914 (2007).
[33] P. Ziherl and S. Svetina, Proc. Natl. Acad. Sci. USA **104**, 761 (2007).
[34] C. Lv, C. Chen, Y. C. Chuang, F. G. Tseng, Y. Yin, F. Grey, and Q. Zheng, Phys. Rev. Lett. **113**, 026101 (2014).
[35] O.-Y. Zhong-can and W. Helfrich, Phys. Rev. A **39**, 5280 (1989).
[36] J.-G. Hu and Z.-c. Ou-Yang, Phys. Rev. E **47**, 461 (1993).